Principles of longitudinal beam diagnostics with coherent radiation

Oliver Grimm and Peter Schmüser, DESY

April 24, 2006

The FLASH facility requires novel techniques to characterize the longitudinal charge distribution of the electron bunches that drive the free-electron laser. Bunch features well below 30 µm need to be resolved. One technique is based on the measurement of the far-infrared radiation spectrum and reconstruction of the bunch shape through Fourier analysis. Currently, experiments using synchrotron, transition and diffraction radiation are operating at FLASH, studying the emission spectra with various instruments. This report describes the basic physics, the measurement principles, and gives explicit mathematical derivations. References to more comprehensive discussions of practical problems and experiments are listed.

After a brief introduction in Sect. 1, the radiation spectrum emitted by an electron bunch is calculated in Sect. 2 in far-field approximation. The technique to reconstruct the bunch shape from the spectrum and its basic limitations are then explained in Sect. 3. Practical examples are given. Some additional material is collected in the appendices.

The typical radiation pulse duration ranges from less than 100 femtoseconds to several picoseconds. Conventional bolometric radiation detectors are far too slow to resolve these short pulses. It is therefore not the instantaneous power that is relevant, but the energy within a pulse. The letter U refers in this report to an energy per unit area, resulting from time integration of the Poynting vector. Frequency is always given as cycle frequency, not angular frequency. The Fourier transform of a function is distinguished from the function itself only by the argument. All calculations are done in SI units.

1 Introduction to coherent radiation diagnostics

The principle of coherent radiation diagnostics is outlined in this introductory section for the special case of synchrotron radiation from circular motion. The angle-integrated energy spectrum of a single relativistic electron with energy E_e moving one turn on a circle with radius R is given by[1] [Jack99]

$$\frac{\mathrm{d}W}{\mathrm{d}\lambda} = \frac{\sqrt{3}e^2}{2\varepsilon_0}\frac{\gamma\lambda_\mathrm{c}}{\lambda^3}\int\limits_{\lambda_\mathrm{c}/\lambda}^{\infty} \mathrm{K}_{5/3}(x)\mathrm{d}x \qquad \text{with} \quad \gamma = \frac{E_\mathrm{e}}{m_e c^2}\,, \quad \lambda_\mathrm{c} = \frac{4\pi R}{3\gamma^3}. \tag{1}$$

$\mathrm{K}_{5/3}$ is a modified Bessel function. A bunch of N electrons does not simply radiate N times this spectral energy but the spectrum is enhanced towards long wavelengths due to coherent emission by a progressively larger fraction of all electrons (see Eq. (6) in the next section). For wavelengths much longer than the bunch length, the bunch behaves as a single macro-particle with charge $-N\,e$, and the radiated power scales with N^2.

[1] It should be noted that Eq. (1) is not valid if the electron traverses only a short arc of a circle [Sal97].

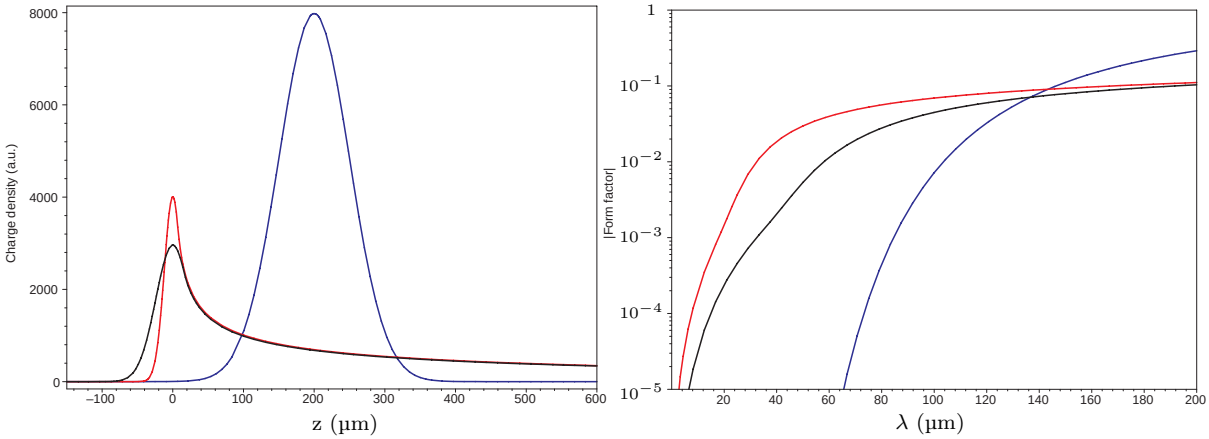

Figure 1 Bunch shapes (left) and absolute magnitude of the corresponding form factors (right). The Gaussian has σ=50 µm. The two shapes with a leading peak and a long tail are computed using a parametrization from [Gel03]. Such bunch shapes are typical for the effect of a magnetic bunch compressor. The form factors are computed according to Eq. (5).

The coherence effect is illustrated for the three electron bunch shapes that are shown in Fig. 1. The figure also shows the corresponding form factors, to be defined in the next section, that determine the coherent amplification. The computed synchrotron radiation spectra for a bunch charge of 1 nC are plotted in Fig. 2. The electron energy is 130 MeV, the radius of curvature is 1.6 m. The spectrum is significantly enhanced in the far-infrared region, and the form of the spectrum depends on the bunch shape. To what extent the bunch shape can be reconstructed from such a spectrum is considered in detail in Sect. 3.1. It is obvious that already the total emitted energy contains information on the longitudinal extension of the bunch.

In practice, the measured spectrum depends not only on the bunch shape, but also on modifications resulting from the suppression of long wavelengths due to cut-off effects in the vacuum chamber, diffraction during radiation transport and frequency-dependent detector response, rendering the reconstruction process quite a demanding task.

2 Radiation spectrum from an electron bunch

The electric field in time-domain produced by a bunch of N electrons is given by the superposition of the fields from the individual electrons,

$$\vec{E}(t) = \sum_{i=1}^{N} \vec{E}_i(t).$$

The spectrum can be calculated by Fourier transformation. The Fourier transform pair[2] used in this report is defined as

$$\vec{E}(\nu) = \int_{-\infty}^{\infty} \vec{E}(t) e^{-2\pi \mathrm{i} \nu t}\, \mathrm{d}t \qquad \text{and} \qquad \vec{E}(t) = \int_{-\infty}^{\infty} \vec{E}(\nu) e^{2\pi \mathrm{i} \nu t}\, \mathrm{d}\nu. \tag{2}$$

We assume that the time-dependence of the individual field contributions from different electrons is identical, except for time-delays corresponding to their spatial separations. Call

[2] If the angular frequency ω is used instead of $2\pi\nu$, a factor $1/\sqrt{2\pi}$ has to be included in front of both integrals.

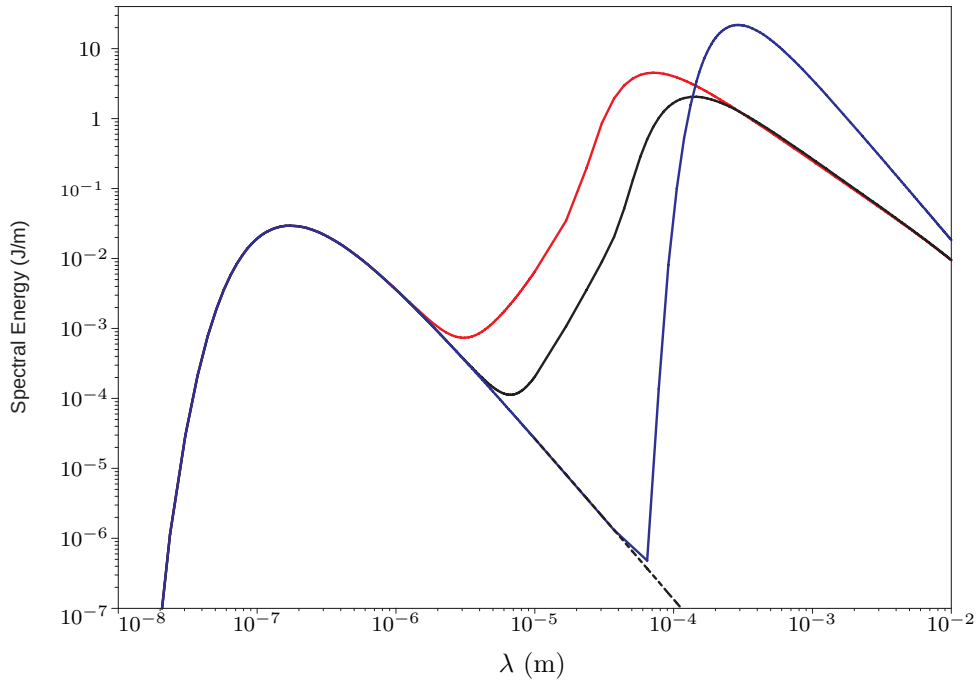

Figure 2 Synchrotron radiation by 130 MeV electrons in a magnet with 1.6 m bending radius. The spectral energy for a bunch charge of 1 nC is shown as a function of wavelength according to Eq. (6). The bunch shapes from Fig. 1 are used. At wavelengths above (10-100) µm a strong enhancement is observed in comparison with the incoherent emission (dashed curve).

$\vec{E}_1(t)$ the field produced by a suitably chosen *reference electron*, then the field of electron i is $\vec{E}_i(t) = \vec{E}_1(t + \Delta t_i)$. The Fourier transform of the total field reads

$$\begin{aligned}\vec{E}(\nu) &= \int_{-\infty}^{\infty} \sum_i \vec{E}_i(t) e^{-2\pi \mathrm{i}\nu t} \mathrm{d}t = \sum_i \int_{-\infty}^{\infty} \vec{E}_1(t + \Delta t_i) e^{-2\pi \mathrm{i}\nu t} \mathrm{d}t = \sum_i \int_{-\infty}^{\infty} \vec{E}_1(\tilde{t}) e^{-2\pi \mathrm{i}\nu(\tilde{t} - \Delta t_i)} \mathrm{d}\tilde{t} \\ &= \sum_i e^{2\pi \mathrm{i}\nu \Delta t_i} \int_{-\infty}^{\infty} \vec{E}_1(\tilde{t}) e^{-2\pi \mathrm{i}\nu \tilde{t}} \mathrm{d}\tilde{t} = \vec{E}_1(\nu) \sum_i e^{2\pi \mathrm{i}\nu \Delta t_i}. \end{aligned} \tag{3}$$

In this equation, the origin of the radiation field is of no importance, it could for example be produced by relativistic electrons that are deflected in a magnetic field (synchrotron radiation) or that cross the boundary between two media of different dielectric properties (transition radiation). What matters is the same time-domain behaviour of all particles, meaning that the electrons are uncorrelated. The present treatment is not applicable to non-stationary situations where the radiation pulse emitted by an electron may be modified by the previously emitted radiation from other electrons. This happens for example at the edge of a magnetic field (see [Sal97] for details). In such cases the assumption of identical pulse shapes is no longer justified.

The energy spectrum in the far-field is calculated in Appendix A, Eq. (18):

$$\frac{\mathrm{d}U}{\mathrm{d}\nu} = \left\langle 2\varepsilon_0 c \left| \vec{E}(\nu) \right|^2 \right\rangle .$$

The angle brackets indicate the ensemble average which must be taken since $\vec{E}(\nu)$ is the field resulting from one particular microscopic distribution of particles while $\mathrm{d}U/\mathrm{d}\nu$ is a macroscopic quantity.

For an electron bunch of arbitrary shape, as depicted in Fig. 3, the time delay between electron i and the reference electron 1 is $\Delta t_i = (R_i - R_1)/c$. The basic assumption that all electrons contribute the same electric field pulse in time-domain except for a time delay defines a far-field condition. In effect, this requires the two unit vectors $\vec{n}$ and $\vec{n}_i$ in Fig. 3 to be parallel. Since $\vec{r}_i + R_i\vec{n}_i = R_1\vec{n}$,

$$R_i = R_1\,\vec{n}\cdot\vec{n}_i - \vec{n}_i\cdot\vec{r}_i \approx R_1 - \vec{n}\cdot\vec{r}_i.$$

The time delay can thus be written as

$$\Delta t_i = -\vec{n}\cdot\vec{r}_i/c = -\vec{k}\cdot\vec{r}_i/(c\,k), \qquad \text{where} \quad \vec{k} = \frac{2\pi}{\lambda}\vec{n}.$$

$\vec{k}$ is the wave vector, pointing from the reference electron to the observation point. The time delay Δt_i leads to a phase shift between the electromagnetic waves emitted from electron i and the reference electron 1 given by $2\pi c\,\Delta t_i/\lambda = -\vec{k}\cdot\vec{r}_i$. The wavelength-dependent energy density spectrum[3] becomes

$$\frac{\mathrm{d}U}{\mathrm{d}\lambda} = \frac{2\varepsilon_0 c^2}{\lambda^2}\left\langle\left|\vec{E}_1(\vec{k})\sum_i e^{-\mathrm{i}\vec{k}\cdot\vec{r}_i}\right|^2\right\rangle = \left(\frac{\mathrm{d}U}{\mathrm{d}\lambda}\right)_1\left\langle\left|\sum_i e^{-\mathrm{i}\vec{k}\cdot\vec{r}_i}\right|^2\right\rangle$$

where

$$\left(\frac{\mathrm{d}U}{\mathrm{d}\lambda}\right)_1 = \frac{2\varepsilon_0 c^2}{\lambda^2}\left|\vec{E}_1(\vec{k})\right|^2$$

is the spectrum radiated by a single electron. Evaluation of the ensemble average yields

$$\begin{aligned}\left\langle\left|\sum_i e^{-\mathrm{i}\vec{k}\cdot\vec{r}_i}\right|^2\right\rangle &= \left\langle\left(\sum_i e^{-\mathrm{i}\vec{k}\cdot\vec{r}_i}\right)\cdot\left(\sum_j e^{\mathrm{i}\vec{k}\cdot\vec{r}_j}\right)\right\rangle \\ &= \sum_{i=1}^{N} 1 + \left\langle\sum_{i=1}^{N}\sum_{\substack{j=1\\ j\neq i}}^{N} e^{-\mathrm{i}\vec{k}\cdot\vec{r}_i}\cdot e^{\mathrm{i}\vec{k}\cdot\vec{r}_j}\right\rangle = N + \left\langle\sum_{i=1}^{N} e^{-\mathrm{i}\vec{k}\cdot\vec{r}_i}\right\rangle\left\langle\sum_{\substack{j=1\\ j\neq i}}^{N} e^{\mathrm{i}\vec{k}\cdot\vec{r}_j}\right\rangle\end{aligned}$$

We now define the normalized three-dimensional particle density distribution by

$$S_{3\mathrm{D}}(\vec{r}) = \frac{1}{N}\left\langle\sum_{i=1}^{N}\delta(\vec{r}-\vec{r}_i)\right\rangle = \frac{1}{N-1}\left\langle\sum_{\substack{j=1\\ j\neq i}}^{N}\delta(\vec{r}-\vec{r}_j)\right\rangle.$$

The equality of the two ensemble averages follows from the fact that the probability distributions of N and N-1 electrons are identical due to our assumption of uncorrelated electrons. With this definition of the particle density the above ensemble average can be written as

$$\left\langle\left|\sum_i e^{-\mathrm{i}\vec{k}\cdot\vec{r}_i}\right|^2\right\rangle = N + N(N-1)\int S_{3\mathrm{D}}(\vec{r})e^{-\mathrm{i}\vec{k}\cdot\vec{r}}\mathrm{d}\vec{r}\cdot\int S_{3\mathrm{D}}(\vec{s})e^{\mathrm{i}\vec{k}\cdot\vec{s}}\mathrm{d}\vec{s}.$$

[3]From the requirement $|(\mathrm{d}U/\mathrm{d}\nu)\mathrm{d}\nu| = |(\mathrm{d}U/\mathrm{d}\lambda)\mathrm{d}\lambda|$, it follows that $\mathrm{d}U/\mathrm{d}\lambda = c/\lambda^2(\mathrm{d}U/\mathrm{d}\nu)$.

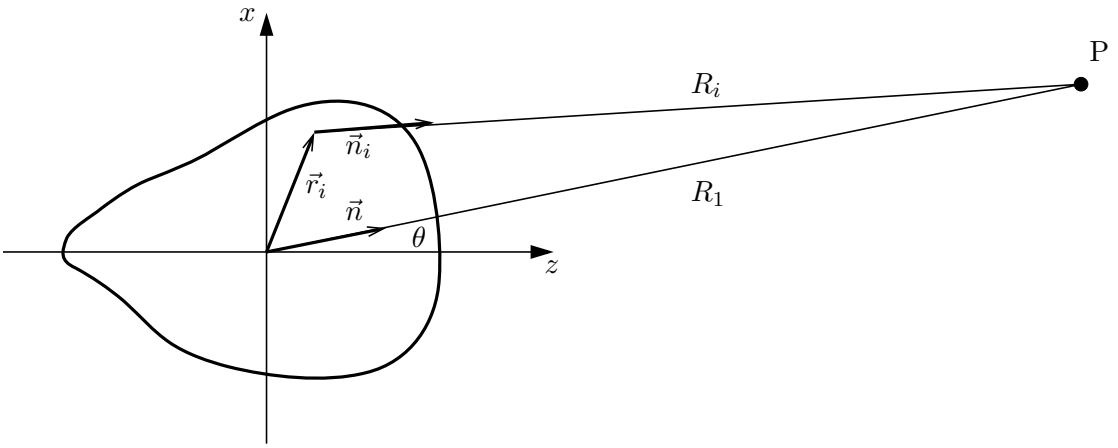

Figure 3 Designations used for describing coherent radiation from a bunch of electrons. The distance to the observation point P is assumed to be large compared to the size of the bunch. Therefore the unit vector $\vec{n}_i$ pointing from electron i to P is nearly parallel to $\vec{n}$ which points from the reference electron 1 at the origin to P.

The three-dimensional *bunch form factor* is defined as the Fourier transform of the three-dimensional normalized particle density distribution

$$F_{3\mathrm{D}}(\vec{k}) = \int S_{3\mathrm{D}}(\vec{r}) e^{-\mathrm{i}\vec{k}\cdot\vec{r}}\,\mathrm{d}\vec{r}. \tag{4}$$

The effect of a finite transverse size will be discussed in Sect. 3.4. Note, however, that experimentally transverse and longitudinal size effects cannot be separated. Sufficient focusing of the electron beam is necessary to suppress transverse effects and to obtain a high longitudinal sensitivity. In the following, only the *longitudinal form factor*

$$\boxed{F(\lambda) = \int_{-\infty}^{\infty} S(z) e^{-2\pi \mathrm{i} z/\lambda}\,\mathrm{d}z} \tag{5}$$

is considered, where the *longitudinal charge distribution* is the projection of the three-dimensional distribution onto the z axis: $S(z) = \int S_{3\mathrm{D}}(\vec{r})\,\mathrm{d}x\mathrm{d}y$. It derives from Eq. (4) if $\vec{k}$ is along the z direction. Using this form factor the radiation spectrum becomes

$$\boxed{\frac{\mathrm{d}U}{\mathrm{d}\lambda} = \left(\frac{\mathrm{d}U}{\mathrm{d}\lambda}\right)_1 \left(N + N(N-1)\,|F(\lambda)|^2\right).} \tag{6}$$

The first term is the incoherent part, proportional the number N of electrons. The second part accounts for coherent emission and is proportional to $N(N-1) \approx N^2$.

The theoretical possibility for a three dimensional (tomographic) bunch shape reconstruction is contained in the freedom of choosing the projection axis. This choice, however, is usually strongly limited by the emission characteristics of the relativistic source, being often tightly collimated in the forward direction. A definite - and within certain limits adjustable - observation angle can be achieved with Čerenkov radiation.

3 Reconstruction of the bunch charge distribution

3.1 Kramers-Kronig relation for phase reconstruction

The reconstruction of the longitudinal particle density distribution $S(z)$ by inverse Fourier transformation is not directly possible because only the magnitude of the form factor can be measured

through Eq. (6) but not its phase. The *Kramers-Kronig relation*[4] can be utilized to determine the phase within certain limitations. The application of the Kramers-Kronig technique to longitudinal bunch shape diagnostics was first suggested by Lai and Sievers [Lai97]. The derivation given here follows the principles outlined in [Woo72].

Since a time shift of the bunch profile results only in an unimportant overall phase factor[5] and the electron bunches are of finite length, the time profile can always be shifted such that $S(z) = 0$ for $z < 0$ without loss of generality. Now the definition of the form factor is extended to the complex frequency domain by defining a complex frequency

$$\nu = \nu_\mathrm{r} + \mathrm{i}\,\nu_\mathrm{i}$$

The exponential function $e^{\mathrm{i}\alpha\nu}$ with a real coefficient α is an analytic function of ν. This can be seen by writing

$$e^{\mathrm{i}\alpha\nu} = u(\nu_\mathrm{r}, \nu_\mathrm{i}) + \mathrm{i}v(\nu_\mathrm{r}, \nu_\mathrm{i}), \qquad u(\nu_\mathrm{r}, \nu_\mathrm{i}) = \cos(\alpha\nu_\mathrm{r})e^{-\alpha\nu_\mathrm{i}}, \;\; v(\nu_\mathrm{r}, \nu_\mathrm{i}) = \sin(\alpha\nu_\mathrm{r})e^{-\alpha\nu_\mathrm{i}},$$

and obtaining

$$\frac{\partial u}{\partial \nu_\mathrm{r}} = -\alpha \sin(\alpha\nu_\mathrm{r})e^{-\alpha\nu_\mathrm{i}} = \frac{\partial v}{\partial \nu_\mathrm{i}}\,, \qquad \frac{\partial u}{\partial \nu_\mathrm{i}} = -\alpha \cos(\alpha\nu_\mathrm{r})e^{-\alpha\nu_\mathrm{i}} = -\frac{\partial v}{\partial \nu_\mathrm{r}}.$$

These are the Cauchy-Riemann equations. Since the partial derivatives are also continuous, the exponential is analytic. In the form factor integral

$$F(\nu) = \int_0^\infty S(z) e^{-2\pi\mathrm{i}\nu z/c}\,\mathrm{d}z \tag{7}$$

the exponential is multiplied with a real function $S(z)$ that does not depend on ν, therefore the form factor $F(\nu)$ is also analytic in the entire complex frequency plane.

The Kramers-Kronig relation connects the real and imaginary part of an analytic function. In many cases, for example for the complex refractive index, either the real or imaginary part can be measured and the relation can then be used directly to deduce the other part. In the present context, however, neither the real nor the imaginary part of the form factor is accessible but only its magnitude. The determination of the phase requires a particular treatment.

We write

$$F(\nu) = \rho(\nu) e^{\mathrm{i}\Theta(\nu)}$$

with real functions $\rho(\nu) \geq 0$ and $\Theta(\nu)$, and take the logarithm:

$$\ln F(\nu) = \ln \rho(\nu) + \mathrm{i}\,\Theta(\nu).$$

[4] In most general terms, the Kramers-Kronig relation connects the real and imaginary part of a response function of a linear, causal system [Toll56]. The connection to the bunch shape reconstruction problem is made by writing Eq. (3) as $\vec{E}(\nu) = NF_\mathrm{3D}(\nu)\vec{E}_1(\nu)$: $\vec{E}_1(\nu)$ is the stimulus, $\vec{E}(\nu)$ the response, and $NF_\mathrm{3D}(\nu)$ the response function. This identification might appear far-fetched, but conceptually the stimulus can be identified with the cause for radiation emission, e.g. the magnetic field for synchrotron radiation or refractive-index changes for transition radiation. Then $\vec{E}(\nu)$ is the response of the bunch to this stimulus.

[5] An overall phase is equivalent to a shift of the longitudinal profile because $\int_{-\infty}^{\infty} S(z)\exp(2\pi\mathrm{i}(\Delta z - z)/\lambda)\,\mathrm{d}z = \int_{-\infty}^{\infty} S(z+\Delta z)\exp(-2\pi\mathrm{i}z/\lambda)\,\mathrm{d}z$. This shift is unobservable since the arrival time of the bunch is *in principle* not accessible via a frequency-domain approach due to the time integration from $-\infty$ to $+\infty$.

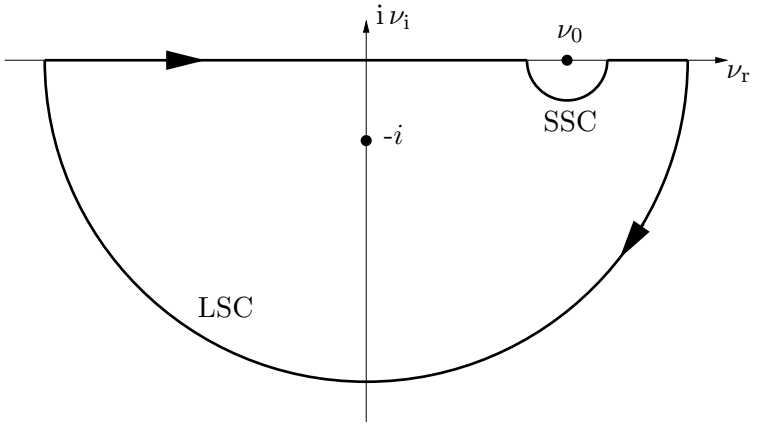

Figure 4 Integration contour C for evaluating the Kramers-Kronig relations by using the residue theorem. The integral over the large semicircle LSC vanishes in the limit of an infinite radius.

The two Cauchy-Riemann equations for $F(\nu)$ require that

$$\left(\frac{\partial\rho}{\partial\nu_\mathrm{r}} - \rho\frac{\partial\Theta}{\partial\nu_\mathrm{i}}\right)\cos\Theta = \left(\frac{\partial\rho}{\partial\nu_\mathrm{i}} + \rho\frac{\partial\Theta}{\partial\nu_\mathrm{r}}\right)\sin\Theta \quad \wedge \quad \left(\frac{\partial\rho}{\partial\nu_\mathrm{i}} + \rho\frac{\partial\Theta}{\partial\nu_\mathrm{r}}\right)\cos\Theta = \left(-\frac{\partial\rho}{\partial\nu_\mathrm{r}} + \rho\frac{\partial\Theta}{\partial\nu_\mathrm{i}}\right)\sin\Theta.$$

By multiplying the first equation with $\cos\Theta$ and the second with $\sin\Theta$ and then subtracting both, the terms in brackets are found to vanish individually.[6] These are just the Cauchy-Riemann equations for $\ln F(\nu)$. Therefore, as long as $\rho(\nu)$ does not vanish, also the logarithm is analytic. This property is used in the following derivations. The effect of zeros in the form factor is considered in Sect. 3.3.

The magnitude $\rho(\nu)$ of the form factor can be derived from the power spectrum Eq. (6) for real positive frequencies. A severe problem arises because the form factor vanishes at high frequencies, as the bunch shape can only contain structures of finite width. The logarithm will then diverge. For this reason an auxiliary function $f(\nu)$ is defined by

$$f(\nu) = \frac{(\nu_0\nu - i^2)\ln F(\nu)}{(\nu^2 - i^2)(\nu_0 - \nu)}\,, \qquad |f(\nu)| = \frac{|\nu_0\nu - i^2|\sqrt{\ln^2\rho(\nu) + \Theta^2(\nu)}}{|\nu^2 - i^2|\cdot|\nu_0 - \nu|},$$

where i in italics is defined by $i = \mathrm{i}\,\mathrm{s}^{-1}$ to be dimensionally correct. The function $f(\nu)$ is a product of analytic functions and as such analytic, except at the isolated singularities at $\nu = \nu_0$ and $\nu = \pm i$.

The residue theorem will now be applied for the closed clockwise contour C shown in Fig. 4:

$$\oint\limits_\mathrm{C} f(\nu)\,\mathrm{d}\nu = \oint\limits_\mathrm{C} \frac{(\nu_0\nu - i^2)\ln F(\nu)}{(\nu + i)(\nu - i)(\nu_0 - \nu)}\,\mathrm{d}\nu = -2\pi\mathrm{i}\frac{(i\nu_0 + i^2)\ln F(-i)}{2i(\nu_0 + i)} = -\mathrm{i}\,\pi\ln F(-i). \quad (8)$$

Due to the assumption that $\rho(\nu)$ does not vanish, the integrand has only one pole at $\nu = -i$ inside the contour. The contour integral can be broken down into integrals over the large semicircle LSC, over the small semicircle SSC and a principal value integral over the real axis, indicated by $\mathcal{P}$:

$$\oint\limits_\mathrm{C} f(\nu)\,\mathrm{d}\nu = \int\limits_\mathrm{LSC} f(\nu)\,\mathrm{d}\nu + \int\limits_\mathrm{SSC} f(\nu)\,\mathrm{d}\nu + \mathcal{P}\int\limits_{-\infty}^{\infty} f(\nu_\mathrm{r})\,\mathrm{d}\nu_\mathrm{r}. \quad (9)$$

[6] Thanks to H. Delsim-Hashemi for pointing this out to us.

The prerequisite that $S(z) = 0$ for $z < 0$ assures that only positive z values appear in Eq. (7). This implies that the form factor $F(\nu)$ is bounded in the lower half plane ($\nu_\mathrm{i} < 0$) by virtue of the real part of the exponential, $\exp(2\pi\nu_\mathrm{i} z/c)$: it vanishes for $\nu_\mathrm{i} \to -\infty$. It also vanishes for $|\nu_\mathrm{r}| \to \infty$ for all practical cases, since the charge distribution will not contain infinitely fine structures, as was already mentioned above. It can thus be assumed that $\rho(\nu)$ drops faster than some negative power at large $|\nu|$,

$$\rho(\nu) < b|\nu|^{-\alpha} \quad \text{for} \quad |\nu| \to \infty,$$

with an exponent $\alpha > 0$. This implies that the contour integral over the large semicircle LSC in the lower half complex plane vanishes in the limit of an infinite radius:

$$\lim_{|\nu|\to\infty} \left| \int\limits_{\mathrm{LSC}} f(\nu)\,\mathrm{d}\nu \right| \le \lim_{|\nu|\to\infty} \int\limits_0^\pi |f(\nu)|\,|\nu|\,\mathrm{d}\varphi = \lim_{|\nu|\to\infty} \frac{\pi\alpha\nu_0 \ln|\nu|}{|\nu|} = 0 \qquad (\nu = |\nu|e^{\mathrm{i}\varphi}). \quad (10)$$

The integral over the small semicircle, which is centered at the real frequency $\nu_0 > 0$, can be evaluated by writing $f(\nu) = g(\nu)/(\nu_0 - \nu)$, where $g(\nu)$ is a continuous function in the vicinity of ν_0, and by setting $\nu_0 - \nu = \epsilon\, e^{\mathrm{i}\varphi}$. In the limit $\epsilon \to 0$ one obtains

$$\int\limits_{\mathrm{SSC}} f(\nu)\,\mathrm{d}\nu \approx g(\nu_0) \int\limits_{\mathrm{SSC}} \frac{1}{\nu_0 - \nu}\,\mathrm{d}\nu = g(\nu_0) \int\limits_\pi^0 \frac{1}{\epsilon e^{\mathrm{i}\varphi}} \epsilon e^{\mathrm{i}\varphi}\,\mathrm{i}\,\mathrm{d}\varphi = \mathrm{i}\pi g(\nu_0) = \mathrm{i}\pi \ln F(\nu_0). \quad (11)$$

Inserting the results from Eq. (8), Eq. (10) and Eq. (11) into Eq. (9) yields

$$\mathcal{P}\int\limits_{-\infty}^{\infty} f(\nu_\mathrm{r})\,\mathrm{d}\nu_\mathrm{r} + \mathrm{i}\pi \ln F(\nu_0) = -\mathrm{i}\pi \ln F(-i).$$

We take the real part of this equation and use the fact that $F(-i)$ is a real number, which follows from Eq. (7). Then, by dropping the index r as from now on only real frequencies are involved,

$$\Theta(\nu_0) = \frac{1}{\pi}\mathcal{P}\int\limits_{-\infty}^{\infty} \frac{(\nu\nu_0 - i^2)\ln\rho(\nu)}{(\nu^2 - i^2)(\nu_0 - \nu)}\,\mathrm{d}\nu.$$

The integration can be restricted to positive frequencies by using the property of the complex form factor Eq. (7) that $F^*(\nu) = F(-\nu)$ for real ν and hence $\rho(-\nu) = \rho(\nu)$, which implies

$$\int\limits_{-\infty}^{0} \frac{(\nu\nu_0 - i^2)\ln\rho(\nu)}{(\nu^2 - i^2)(\nu_0 - \nu)}\,\mathrm{d}\nu = \int\limits_0^{\infty} \frac{(-\nu\nu_0 - i^2)\ln\rho(\nu)}{(\nu^2 - i^2)(\nu_0 + \nu)}\,\mathrm{d}\nu.$$

The result is

$$\Theta(\nu_0) = \frac{2\nu_0}{\pi}\mathcal{P}\int\limits_0^{\infty} \frac{\ln\rho(\nu)}{\nu_0^2 - \nu^2}\,\mathrm{d}\nu.$$

The singularity at ν_0 can be removed by subtracting the vanishing quantity

$$\frac{2\nu_0}{\pi}\mathcal{P}\int\limits_0^{\infty} \frac{\ln\rho(\nu_0)}{\nu_0^2 - \nu^2}\,\mathrm{d}\nu \quad = \quad \frac{2\nu_0 \ln\rho(\nu_0)}{\pi} \lim_{\epsilon\to 0} \left(\int\limits_0^{\nu_0-\epsilon} \frac{1}{\nu_0^2 - \nu^2}\,\mathrm{d}\nu + \int\limits_{\nu_0+\epsilon}^{\infty} \frac{1}{\nu_0^2 - \nu^2}\,\mathrm{d}\nu \right)$$

$$= \frac{\ln\rho(\nu_0)}{\pi}\lim_{\epsilon\to 0}\left(\ln\frac{\nu_0+\nu}{\nu_0-\nu}\Big|_0^{\nu_0-\epsilon} + \ln\frac{\nu_0+\nu}{\nu-\nu_0}\Big|_{\nu_0+\epsilon}^{\infty}\right) = 0.$$

Finally, the Kramers-Kronig relation for phase reconstruction of the form factor becomes

$$\boxed{\Theta(\nu_0) = \frac{2\nu_0}{\pi}\int_0^\infty \frac{\ln(\rho(\nu)/\rho(\nu_0))}{\nu_0^2-\nu^2}\,\mathrm{d}\nu.} \tag{12}$$

There is indeed no longer a singularity at $\nu = \nu_0$, as can be verified by a Taylor expansion of $\ln\rho(\nu)$ about ν_0 (unless $\rho(\nu_0)$ vanishes, in which case the phase is meaningless).

The longitudinal bunch charge distribution follows from the inverse Fourier integral Eq. (5)

$$\begin{aligned} S(z) &= \frac{1}{c}\int_{-\infty}^{\infty} F(\nu)e^{2\pi\mathrm{i}\nu z/c}\mathrm{d}\nu = \frac{1}{c}\int_0^\infty \left(F(\nu)e^{2\pi\mathrm{i}\nu z/c} + F(-\nu)e^{-2\pi\mathrm{i}\nu z/c}\right)\mathrm{d}\nu \\ &= \frac{1}{c}\int_0^\infty \left(F(\nu)e^{2\pi\mathrm{i}\nu z/c} + F^*(\nu)e^{-2\pi\mathrm{i}\nu z/c}\right)\mathrm{d}\nu \end{aligned}$$

Hence

$$\boxed{S(z) = \frac{2}{c}\int_0^\infty \rho(\nu)\cos\left(\frac{2\pi\nu}{c}z + \Theta(\nu)\right)\mathrm{d}\nu.} \tag{13}$$

The integration extends over all frequencies from zero to infinity. As any measurement will cover only a limited range, suitable extrapolations to small and large frequencies are usually needed in practice.

The normalized time profile $S_\mathrm{t}(t)$ of the electron bunch follows by using $z = ct$, valid for highly relativistic particles:

$$S_\mathrm{t}(t) = 2\int_0^\infty \rho(\nu)\cos\left(2\pi\nu\, t + \Theta(\nu)\right)\mathrm{d}\nu. \tag{14}$$

3.2 Practical examples for bunch shape reconstructions

To illustrate the applicability of the phase reconstruction technique, examples are given in Fig. 5 for three bunch shapes: a Gaussian with σ_z=300 µm, a double Gaussian with $\sigma_{z,1}$=50 µm and $\sigma_{z,2}$=300 µm, and a bunch with a Gaussian head (σ_z=50 µm) and an exponential tail (1 mm decay length). The form factors were calculated for 500 frequencies between a lower value of 100 GHz or 400 GHz, respectively, and an upper value of 5 THz. Using the absolute values of the theoretical form factors, the phases were determined according to Eq. (12) and the shapes were reconstructed with Eq. (13). A simple low-frequency extrapolation $\rho(\nu) = \exp(-\alpha\nu^2)$ was used, with α chosen to join smoothly the data at 100 GHz or 400 GHz, respectively. No high-frequency extrapolation was applied. As can be seen from the figure, the reconstruction works well for all shapes if the lower frequency cut-off of 100 GHz is used. However, severe distortions occur for a lower frequency limit at 400 GHz, except for the 300 µm simple Gaussian bunch for which the Gaussian extrapolation is obviously very good.

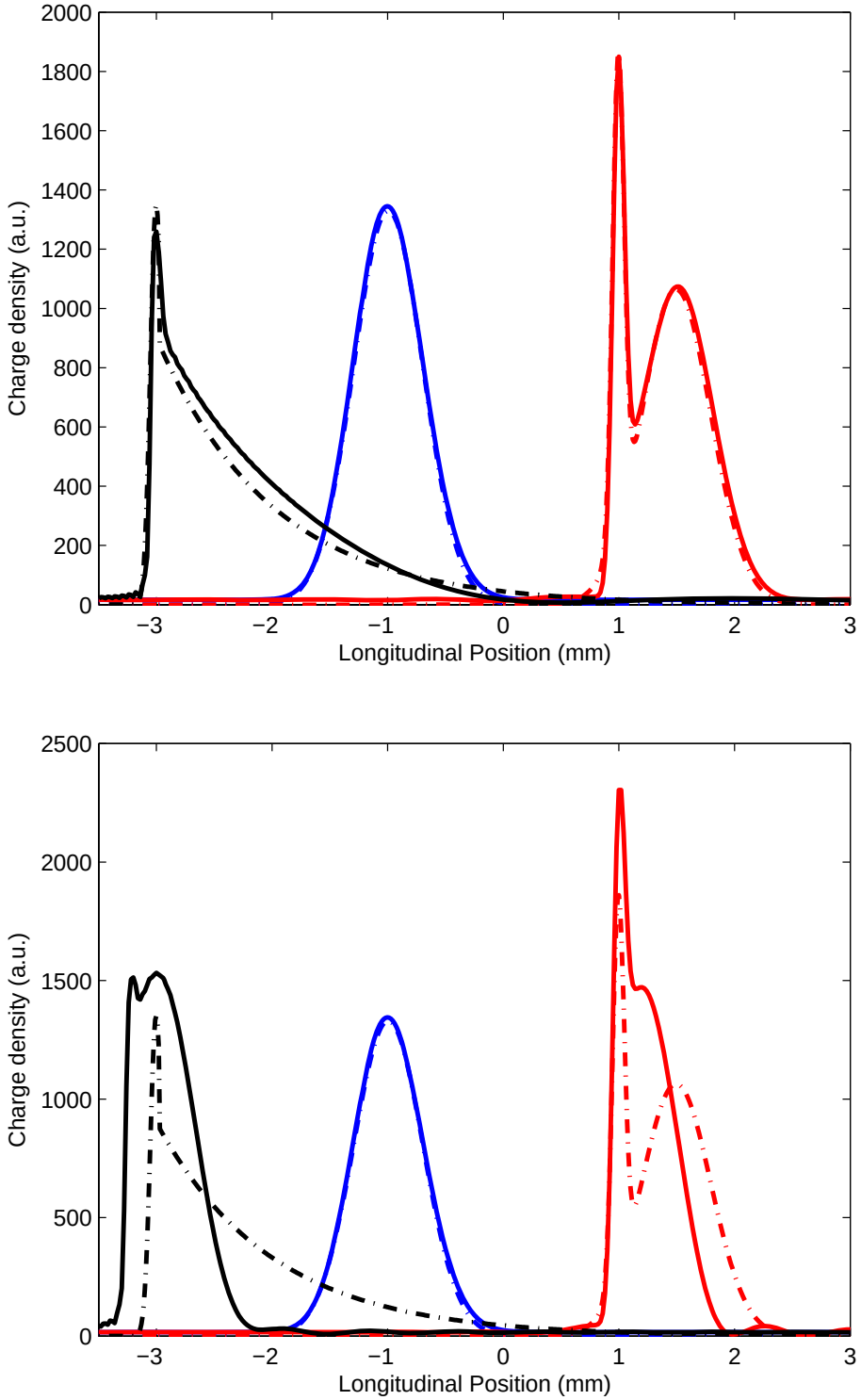

Figure 5 Original (dash-dot) and reconstructed (solid) bunch shapes. The low-frequency extrapolation is $\rho(\nu) = \exp(-\alpha\nu^2)$, joined at 100 GHz on the top and at 400 GHz on the bottom. The curves are shifted horizontally such that their maximum values coincide.

Low- and high-frequency extrapolations are considered in more detail in [Frö05], the effect of measurement noise is studied in [Men05].

If additional time-domain data on the bunch shape are available from an instrument with the resolution function $\mathcal{I}(t)$, the experimentally measured shape $S_{\mathrm{meas}}(t)$ is related to the true shape $S(t)$ by a convolution integral,

$$S_{\mathrm{meas}}(t) = \int S(t')\mathcal{I}(t-t')\,\mathrm{d}t'.$$

In frequency domain this is written as the product of the Fourier transforms,

$$S_{\mathrm{meas}}(\nu) = F(\nu)\mathcal{I}(\nu),$$

where Eq. (7) has been used. The Fourier transform of the measured shape is almost equal to the form factor if $\mathcal{I}(\nu)$ is close to unity. In this case, the low-frequency extrapolation can be replaced by measured data. Assuming for the resolution function a Gaussian with width σ_{instr}, the measuring instrument will act as a low-pass filter, with $\mathcal{I}(\nu)$ dropping to $1/e$ at the frequency $c/(\sqrt{2}\pi\sigma_{\mathrm{instr}})$. For a streak camera with 200 fs rms resolution, for example, this frequency is 800 GHz.

3.3 On zeros in the form factor

An essential prerequisite in the Kramers-Kronig analysis is the absence of zeros in the form factor. This is true for a Gaussian bunch whose form factor is also of Gaussian shape and vanishes nowhere in the complex ν plane. However, already a truncated Gaussian charge distribution possesses a form factor containing zeros. The existence of zeros can therefore not be excluded for realistic bunch shapes.

Suppose the form factor has a simple zero at some complex frequency in the lower half plane, $\mu = \mu_{\mathrm{r}} + \mathrm{i}\,\mu_{\mathrm{i}}$ with $\mu_{\mathrm{i}} < 0$. Then the new function

$$\tilde{F}(\nu) = F(\nu) \cdot \frac{\nu - \mu^*}{\nu - \mu}$$

will be nonzero at $\nu = \mu$. It will be shown below that $\tilde{F}(\nu)$ and $F(\nu)$ have the same magnitude on the real axis.

Let us now admit an arbitrary number zeros of the form factor and label them by μ_n. A new form factor without zeros is defined by

$$\tilde{F}(\nu) = F(\nu) \prod_n B_n(\nu) \quad \text{with} \quad B_n(\nu) = \frac{\nu - \mu_n^*}{\nu - \mu_n}.$$

We have shifted all zeros μ_n of the original form factor into the product which is called the *Blaschke product*[7]. The magnitude of each term is

$$|B_n(\nu)| = \sqrt{\frac{|\nu|^2 + |\mu_n|^2 - 2(\nu_{\mathrm{r}}\mu_{n,\mathrm{r}} - \nu_{\mathrm{i}}\mu_{n,\mathrm{i}})}{|\nu|^2 + |\mu_n|^2 - 2(\nu_{\mathrm{r}}\mu_{n,\mathrm{r}} + \nu_{\mathrm{i}}\mu_{n,\mathrm{i}})}}.$$

On the real frequency axis (ν_{i}=0) the form factor magnitude is not changed by the Blaschke product since $|B_n(\nu)|$=1, and therefore $\rho(\nu) = |F(\nu)| = |\tilde{F}(\nu)|$. Furthermore, $|B_n(\nu)| < 1$ in the

[7] The Blaschke product obviously cannot remove zeros which are on the real frequency axis. Such zeros of the form factor where $\rho(\nu) = 0$, however, do not contribute to the reconstructed bunch shape according to Eq. (13).

lower half plane ($\nu_\mathrm{i} < 0$), so $\tilde{F}(\nu)$ remains bounded. The Kramers-Kronig treatment can thus be applied to the new, zeroless form factor $\tilde{F}(\nu)$. For a rigorous proof that indeed all zeros of the form factor can be absorbed into the Blaschke product see the references quoted in [Toll56].

On the real frequency axis the Blaschke product has unity modulus and can therefore be expressed as a phase factor $\exp(\mathrm{i}\Theta_\mathrm{B}(\nu))$. The real phase is given by

$$\Theta_\mathrm{B}(\nu) = \sum_n \arctan \frac{\Im(B_n(\nu))}{\Re(B_n(\nu))} = \sum_n \arctan \frac{2\mu_{n,\mathrm{i}}(\nu - \mu_{n,\mathrm{r}})}{(\nu - \mu_{n,\mathrm{r}})^2 - \mu_{n,\mathrm{i}}^2}. \tag{15}$$

This *Blaschke phase* is a monotonic function of frequency. To see this consider a single term $B_n(\nu)$ and suppress the subscript n for brevity:

$$\frac{\mathrm{d}}{\mathrm{d}\nu}\left(\frac{2\mu_\mathrm{i}(\nu - \mu_\mathrm{r})}{(\nu - \mu_\mathrm{r})^2 - \mu_\mathrm{i}^2}\right) = -2\mu_\mathrm{i}\frac{(\nu - \mu_\mathrm{r})^2 + \mu_\mathrm{i}^2}{\left((\nu - \mu_\mathrm{r})^2 - \mu_\mathrm{i}^2\right)^2} > 0 \quad \text{for} \quad \mu_\mathrm{i} < 0.$$

Hence also $\mathrm{d}\Theta_B/\mathrm{d}\nu > 0$ for all real frequencies ν, provided the imaginary part of μ is negative.

A further restriction on the contribution from the Blaschke product results from a symmetry of the complex form factor that follows from Eq. (7): $F^*(-\nu^*) = F(\nu)$. A zero located at μ requires always another one at $-\mu^*$ (mirrored at the imaginary frequency axis). The phase contribution from such a pair is

$$\Theta_\mathrm{pair}(\nu) = \arctan \frac{4\nu\mu_\mathrm{i}\left(\nu^2 - |\mu|^2\right)}{\nu^4 + |\mu|^4 - 2\nu^2\mu_\mathrm{r}^2 - 6\nu^2\mu_\mathrm{i}^2}.$$

If $|\mu| \gg |\nu|$, $\Theta_\mathrm{pair}(\nu) \approx 4\mu_\mathrm{i}\nu/|\mu|^2$. A contribution proportional to frequency corresponds, according to Eq. (13), to a mere shift of the reconstructed profile, given here by $2c\mu_\mathrm{i}/(\pi|\mu|^2)$. For this reason, only complex zeros which are not too far away from the frequency range used for the reconstruction contribute to the bunch shape.

We have seen that the Blaschke product leaves the function $\rho(\nu)$ invariant on the real axis. Therefore it is not possible to deduce the Blaschke contribution from a measurement of the absolute value of the form factor. This is the deeper reason why the phase of the form factor and thereby the bunch shape cannot be uniquely reconstructed from spectral intensity measurements only. The Kramers-Kronig phase Eq. (12) is sometimes referred to as the *canonical phase* or the *minimal phase*.

To investigate the influence of zeros in the form factor we consider a σ_z =300 µm Gaussian with a superimposed sinusoidal oscillation. The mathematical procedure is described in Appendix D. The form factor is found to contain infinitely many zeros in the lower half of the complex frequency plane. The Blaschke phase has been computed numerically, see Fig. 10 in the Appendix. Here we restrict our analysis to a computation of the Kramers-Kronig phase Eq. (12) and disregard the zeros in the form factor. Fig. 6 shows that the original particle distribution is well reproduced if just the Kramers-Kronig phase is used in Eq. (13) and the Blaschke phase is ignored. The modification of the bunch shape by the Blaschke phase is not very important and has in practice certainly much less influence than the uncertainties which are due to measurement errors and the low- and high-frequency extrapolations of the measured spectral data.

3.4 Transverse size effects

The form factor for a general three-dimensional charge distribution was calculated in Sect. 2 in far-field approximation, see Eq. (4). Assuming for illustrative purposes that the charge distrib-

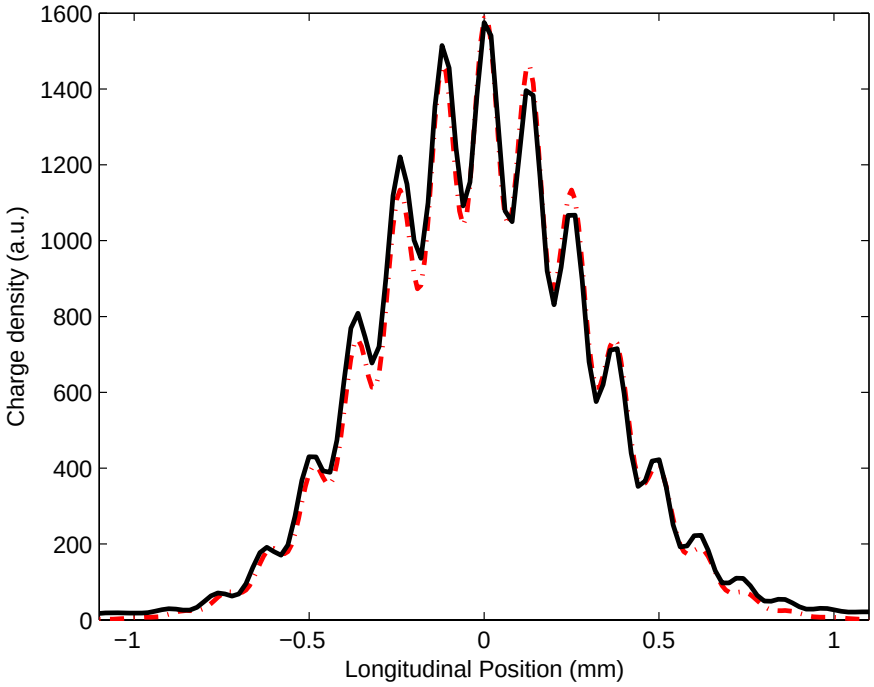

Figure 6 Original (dash-dot) and reconstructed (solid) bunch shape for a Gaussian with a superimposed sinusoidal oscillation. A low-frequency extrapolation $\rho(\nu) = \exp(-\alpha\nu^2)$ is joined at 100 GHz.

ution can be written in product form[8], the form factor can also be factorized. For the case of a longitudinal and transverse Gaussian distribution with rotational symmetry about the z axis,

$$S_{3D}(x,y,z) = \frac{1}{2\pi\sigma_t^2}\exp\left(-\frac{x^2+y^2}{2\sigma_t^2}\right)\frac{1}{\sqrt{2\pi}\sigma_z}\exp\left(-\frac{z^2}{2\sigma_z^2}\right),$$

evaluating Eq. (4) yields

$$\begin{aligned} F_{3D}(k_x,k_y,k_z) &= \frac{1}{\sqrt{2\pi}\sigma_z}\frac{1}{2\pi\sigma_t^2}\int_{-\infty}^{\infty}\!\!\iint \exp\left(-\frac{z^2}{2\sigma_z^2}-\frac{x^2+y^2}{2\sigma_t^2}-\mathrm{i}\left(k_x x+k_y y+k_z z\right)\right)\mathrm{d}x\mathrm{d}y\mathrm{d}z \\ &= \exp\left(-\frac{\sigma_z^2 k_z^2}{2}\right)\exp\left(-\frac{\sigma_t^2(k_x^2+k_y^2)}{2}\right), \end{aligned} \tag{16}$$

where

$$\sqrt{k_x^2+k_y^2} = \frac{2\pi}{\lambda}\sin\theta, \quad k_z = \frac{2\pi}{\lambda}\cos\theta,$$

for an observation angle θ with respect to the z axis. This three-dimensional form factor is plotted in Fig. 7 for four values of σ_t and two values of θ. The form factor is reduced to $1/e$ of its maximum value (obtained for an infinitely thin line bunch) for a transverse size $\sigma_t = \lambda/(\sqrt{2}\pi\sin\theta)$.

[8]This is a good assumption in a straight linac for relativistic electrons with no longitudinal motion and decoupled transverse betatron oscillations. However, if bunch compressors with magnetic chicanes are installed, as for FLASH, this factorization is not necessarily possible.

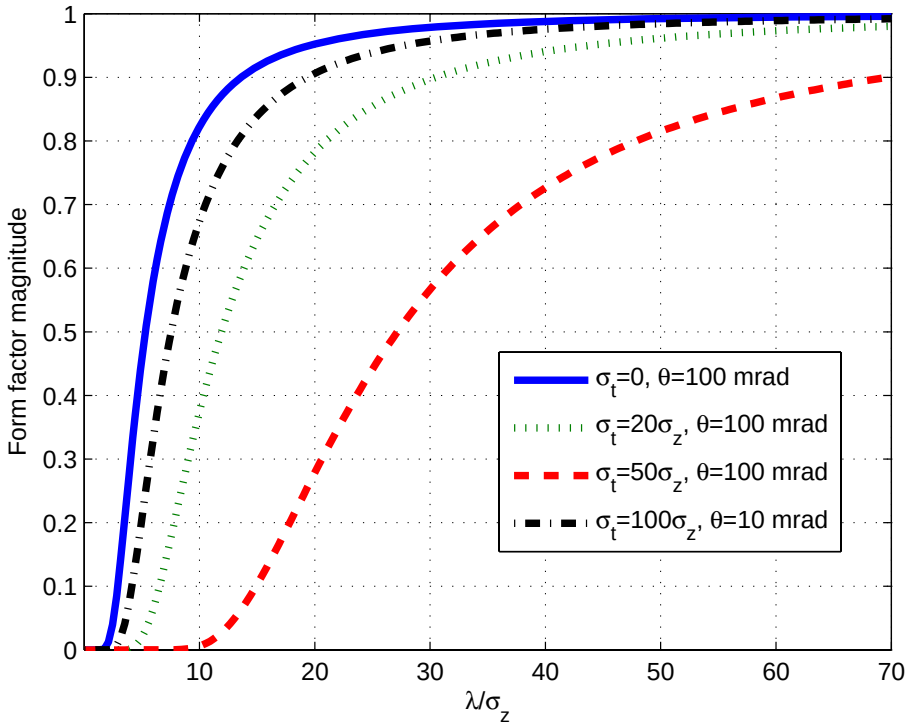

Figure 7 Influence of the transverse bunch size σ_t on the form factor after Eq. (16).

Eq. (16) shows that the transverse contribution to the form factor is determined by $\sigma_\mathrm{t} \sin\theta$, the longitudinal contribution by $\sigma_\mathrm{z} \cos\theta$. For small angles, transverse effects are strongly suppressed. This is generally the case for radiation from highly relativistic electrons which is inevitably strongly collimated, typical opening angles being $\theta \approx 1/\gamma \ll 1$ for transition or synchrotron radiation.

This suppression effect can also be seen from Fig. 3: the path length difference from electron 1 and electron i to the observation point P is given by $\vec{n} \cdot \vec{r}_i = x_i \sin\theta + z_i \cos\theta$, showing again the weak influence of the transverse size for small angles. This argument is valid in general for any charge distribution, also if it cannot be factorized. Although the form factor is rather insensitive to the transverse structure of the electron bunch, the bunches should nevertheless be well focused if fine details of the longitudinal charge distribution shall be resolved.

A Derivation of the frequency spectrum

The energy density spectrum $\mathrm{d}U/\mathrm{d}\nu$ (in units of $\mathrm{J/(Hz\,m^2)}$) at a given position[9] is related to the power density $\mathrm{d}U/\mathrm{d}t$ through

$$U_\mathrm{total} = \int_0^\infty \frac{\mathrm{d}U}{\mathrm{d}\nu}\,\mathrm{d}\nu = \int_{-\infty}^\infty \frac{\mathrm{d}U}{\mathrm{d}t}\,\mathrm{d}t, \tag{17}$$

[9] As the unit indicates, this and the following quantities are taken per unit area, thus they should read in full $\mathrm{d}^2U/\mathrm{d}\nu\mathrm{d}A$. The differential $\mathrm{d}A$ is suppressed for brevity, as well as the variable $\vec{r}$: $\vec{E}(\vec{r},t) \equiv \vec{E}(t)$, etc.

where U_{total} is the energy density (in units of J/m^2). The power density is the absolute magnitude of the Poynting vector $\vec{S}(t)$, [$\vec{S}$]=W/m^2, which in free space is [Jack99]

$$\vec{S}(t) = \frac{1}{\mu_0}\vec{E}(t)\times\vec{B}(t) = \varepsilon_0 c\left((\vec{E}(t))^2\vec{n}(t) - (\vec{E}(t)\cdot\vec{n}(t))\vec{E}(t)\right).$$

For the second equation the relation $\vec{B}(t) = \frac{1}{c}\vec{n}(t)\times\vec{E}(t)$ has been used which is valid in general for the radiation of a single accelerated charge, with $\vec{n}(t)$ the unit vector from the position of the charge at retarded time to the observation point. At large distance from the source, the second term on the right side is absent since then $\vec{E}(t)$ is perpendicular to $\vec{n}(t)$. With this far-field condition,

$$\begin{aligned}
U_{\text{total}} &= \varepsilon_0 c \int_{-\infty}^{\infty} \left|\vec{E}(t)\right|^2 \mathrm{d}t = \varepsilon_0 c \int_{-\infty}^{\infty} \left| \int_{-\infty}^{\infty} \vec{E}(\nu) e^{2\pi \mathrm{i}\nu t} \mathrm{d}\nu \right|^2 \mathrm{d}t \\
&= \varepsilon_0 c \int_{-\infty}^{\infty}\int_{-\infty}^{\infty} \vec{E}(\nu) e^{2\pi \mathrm{i}\nu t}\mathrm{d}\nu \cdot \int_{-\infty}^{\infty} \vec{E}^*(\nu') e^{-2\pi \mathrm{i}\nu' t}\mathrm{d}\nu'\mathrm{d}t \\
&= \varepsilon_0 c \iint_{-\infty}^{\infty} \vec{E}(\nu)\cdot\vec{E}^*(\nu') \int_{-\infty}^{\infty} e^{-2\pi \mathrm{i}(\nu'-\nu)t}\mathrm{d}t\mathrm{d}\nu\mathrm{d}\nu' \\
&= \varepsilon_0 c \iint_{-\infty}^{\infty} \vec{E}(\nu)\cdot\vec{E}^*(\nu')\delta(\nu'-\nu)\mathrm{d}\nu\mathrm{d}\nu' = \varepsilon_0 c \int_{-\infty}^{\infty} |\vec{E}(\nu)|^2 \mathrm{d}\nu = 2\varepsilon_0 c \int_{0}^{\infty} |\vec{E}(\nu)|^2 \mathrm{d}\nu.
\end{aligned}$$

In the last step $\vec{E}^*(-\nu) = \vec{E}(\nu)$ was used, valid since $\vec{E}(t)$ is real. Comparing with Eq. (17),

$$\boxed{\frac{\mathrm{d}U}{\mathrm{d}\nu} = 2\varepsilon_0 c|\vec{E}(\nu)|^2.} \tag{18}$$

B Basic operation principle of an interferometer

One standard instrument for measuring frequency spectra is the interferometer. The basic operation principle of such a device is described in this section for the example of a Michelson interferometer. It is in essence a proof of the Wiener-Khinchin theorem.

The layout of a Michelson interferometer with the relations of electric field before and after the beam splitter is sketched in Fig. 8. A perfect splitter is assumed, dividing the incoming power in two equal parts. Thus the electric field amplitudes of the two outgoing beams are smaller by a factor of $\sqrt{2}$ than the incoming. Due to the symmetric beam splitter characteristic, on average half the intensity is reflected back to the source, as will be shown below.

The time dependent electric field reaching the detector $E_{\text{out}}(t)$ is therefore related to the incoming field $E_{\text{in}}(t)$ by

$$E_{\text{out}}(t) = \frac{E_{\text{in}}(t)}{\sqrt{4}} + \frac{E_{\text{in}}(t - 2\Delta x/c)}{\sqrt{4}}.$$

A slow detector that integrates the instantaneous intensity over the radiation pulse will measure an energy U_{out} as function of mirror displacement Δx (the interferogram) given by

$$U_{\text{out}}(\Delta x) = \int_{-\infty}^{\infty} \varepsilon_0 c\,|E_{\text{out}}(t)|^2\,\mathrm{d}t$$

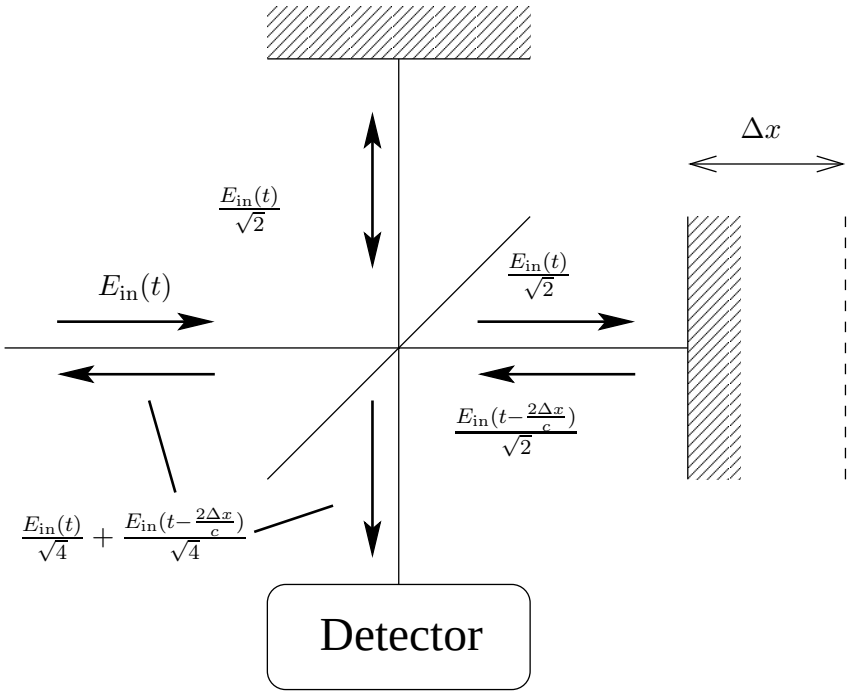

Figure 8 Sketch of the electric field relations in an interferometer

$$
\begin{aligned}
&= \varepsilon_0 c \int_{-\infty}^{\infty} \frac{E_{\rm in}^2(t)}{4} + \frac{E_{\rm in}^2(t-2\Delta x/c)}{4} + \frac{1}{2} E_{\rm in}(t) E_{\rm in}(t-2\Delta x/c)\, {\rm d}t \\
&= \frac{U_{\rm in}}{2} + \frac{\varepsilon_0 c}{2} \int_{-\infty}^{\infty} \int_{-\infty}^{\infty} E_{\rm in}(\nu) e^{2\pi {\rm i}\nu t} {\rm d}\nu \int_{-\infty}^{\infty} E_{\rm in}(\nu') e^{2\pi {\rm i}\nu'(t-2\Delta x/c)} {\rm d}\nu'\, {\rm d}t \\
&= \frac{U_{\rm in}}{2} + \frac{\varepsilon_0 c}{2} \int_{-\infty}^{\infty} \int_{-\infty}^{\infty} E_{\rm in}(\nu) E_{\rm in}(\nu') e^{-4\pi {\rm i}\nu'\Delta x/c} \int_{-\infty}^{\infty} e^{2\pi {\rm i}(\nu+\nu')t}\, {\rm d}t\, {\rm d}\nu' {\rm d}\nu \\
&= \frac{U_{\rm in}}{2} + \frac{\varepsilon_0 c}{2} \int_{-\infty}^{\infty} \int_{-\infty}^{\infty} E_{\rm in}(\nu) E_{\rm in}(\nu') e^{-4\pi {\rm i}\nu'\Delta x/c}\, \delta(\nu+\nu')\, {\rm d}\nu' {\rm d}\nu \\
&= \frac{U_{\rm in}}{2} + \frac{\varepsilon_0 c}{2} \int_{-\infty}^{\infty} E_{\rm in}(\nu) E_{\rm in}(-\nu) e^{4\pi {\rm i}\nu\Delta x/c}\, {\rm d}\nu \\
&= \frac{U_{\rm in}}{2} + \frac{\varepsilon_0 c}{2} \int_{-\infty}^{\infty} |E_{\rm in}(\nu)|^2\, e^{4\pi {\rm i}\nu\Delta x/c}\, {\rm d}\nu \\
&= \frac{U_{\rm in}}{2} + \frac{1}{4} \int_{-\infty}^{\infty} \left(\frac{{\rm d}U}{{\rm d}\nu}\right)_{\rm in} e^{4\pi {\rm i}\nu\Delta x/c}\, {\rm d}\nu \qquad \text{(from Eq. (18))} \\
&= \frac{U_{\rm in}}{2} + \frac{1}{2} \int_{0}^{\infty} \left(\frac{{\rm d}U}{{\rm d}\nu}\right)_{\rm in} \cos\left(\frac{4\pi\nu\Delta x}{c}\right) {\rm d}\nu. \qquad (19)
\end{aligned}
$$

The Fourier transform relation between $E_{\mathrm{in}}(\nu)$ and $E_{\mathrm{in}}(t)$ is defined through Eq. (2). The last line follows from the symmetry of $(\mathrm{d}U/\mathrm{d}\nu)_{\mathrm{in}}$. The units of $U_{\mathrm{out}}(\Delta x)$ and U_{in} are $\mathrm{J/m^2}$.

Apart from the constant offset at $U_{\mathrm{in}}/2$, the interferogram is the cosine Fourier transform of the incoming frequency spectrum which can therefore be recovered by the inverse transform. The Fourier transforms are real, therefore no phase-retrieval problems occur as for the bunch shape reconstruction in Sect. 3.1.

The integral averaged over Δx vanishes, so the detector sees only half of the incoming intensity, the other half is reflected back to the source.

A Martin-Puplett interferometer works along the same principles, but no radiation that enters the device is going back to the source[10], allowing an easy removal of intensity fluctuations. The difference interferogram of the two detectors shows no offset. Consult [Frö05] for detailed information on theoretical background and on practicalities.

C Interferogram of a Gaussian bunch

The form factor $F(\lambda)$ of a Gaussian line bunch with normalized longitudinal charge distribution

$$S(z) = \frac{1}{\sqrt{2\pi}\sigma} \exp\left(-\frac{z^2}{2\sigma^2}\right)$$

is, from Eq. (5),

$$F(\lambda) = \exp\left(-\frac{2\pi^2\sigma^2}{\lambda^2}\right).$$

In the following, the number of particles is assumed to be large so that the coherent part of the total emission spectrum Eq. (6) dominates.

Taking first a single-electron spectrum $(\mathrm{d}U/\mathrm{d}\lambda)_{\mathrm{in}}$ independent of λ, for example from transition radiation, the interferogram from Eq. (19) will be Gaussian,

$$U_{\mathrm{out}}(\Delta x) - \frac{U_{\mathrm{in}}}{2} \sim \exp\left(-\frac{\Delta x^2}{2\left(\sigma/\sqrt{2}\right)^2}\right),$$

with a width a factor of $\sqrt{2}$ smaller than the width of the charge distribution.

As second example the spectrum of synchrotron radiation from circular motion is used. In the forward direction for long wavelengths[11] $\lambda \gg \lambda_{\mathrm{c}}$ it is given by [Jack99]

$$\left(\frac{\mathrm{d}U}{\mathrm{d}\lambda}\right)_{\mathrm{in}} = \frac{3^{1/3}e^2}{2\varepsilon_0}\frac{1}{d^2\lambda^2}\left(\frac{\Gamma(2/3)}{\pi}\right)^2\left(\frac{\pi R}{\lambda}\right)^{2/3} \sim \lambda^{-\frac{8}{3}},$$

where Γ denotes the Gamma function and d is the distance to the observation point. Here, the interferogram will be

$$U_{\mathrm{out}}(\Delta x) - \frac{U_{\mathrm{in}}}{2} \sim \int_0^\infty \nu^{2/3} \exp\left(-\frac{4\pi^2\sigma^2\nu^2}{c^2}\right) \cos\left(\frac{4\pi\nu\Delta x}{c}\right) \mathrm{d}\nu.$$

This cannot be evaluate analytically. In Fig. 9, a comparison of this case with that of a flat single electron spectrum for a Gaussian bunch with σ=300 µm is shown. A dip appears for the synchrotron radiation case and the full width at half maximum is decreased by about 30% compared to the flat spectrum.

[10] However, since linearly polarized radiation is needed, an input polarizer is used. For unpolarized radiation, half of the intensity is still lost, but independent of the mirror position Δx.

[11] For the parameters used in Fig. 2, $\lambda_{\mathrm{c}} = 409\,\mathrm{nm}$.

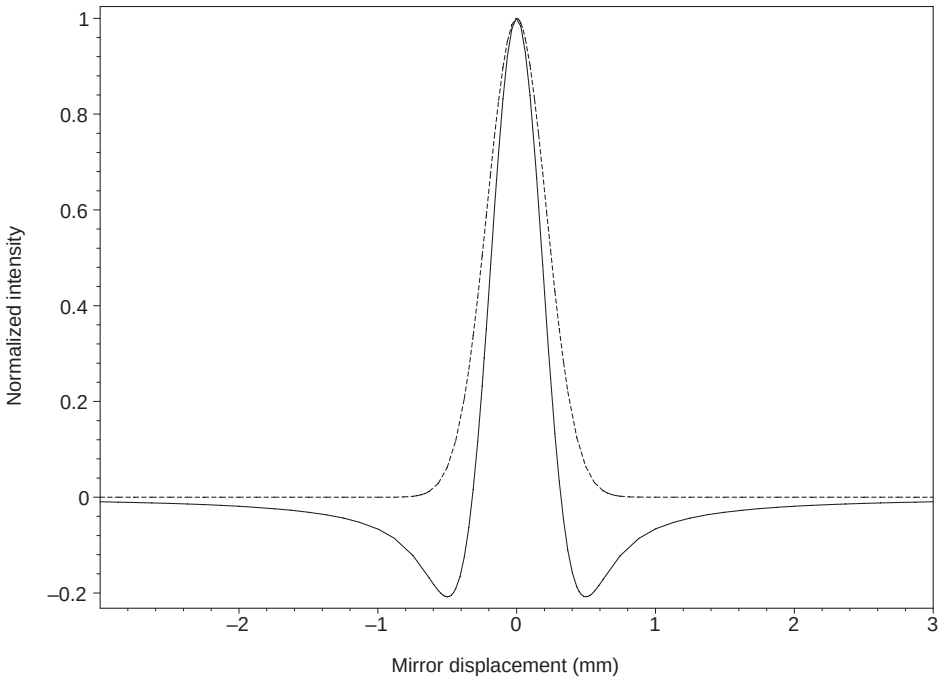

Figure 9 Normalized interferograms for a Gaussian bunch with σ=300 µm and far-infrared synchrotron radiation (solid line) or flat (dashed line) single electron spectrum.

D A form factor with complex zeros

Consider a charge distribution consisting of a Gaussian with a sine-like oscillation of modulation $1/p$, $p > 0$, and modulation wavelength λ_0,

$$S(z) = \frac{1}{\sqrt{2\pi}\sigma} \exp\left(\frac{-z^2}{2\sigma^2}\right) \left(1 - \frac{1}{p} \exp\left(\frac{-\sigma^2}{2\lambda_0^2}\right) + \frac{1}{p} \cos\frac{z}{\lambda_0}\right), \tag{20}$$

which in this form is correctly normalized according to Sect. 2. It is non-negative for all z as long as

$$p \geq \exp\left(\frac{-\sigma^2}{2\lambda_0^2}\right) + 1. \tag{21}$$

The corresponding form factor is

$$\begin{aligned} F(\nu) &= \int_{-\infty}^{\infty} S(z) \exp\left(\frac{-2\pi \mathrm{i}\nu}{c} z\right) \mathrm{d}z \\ &= \frac{\sqrt{2}}{\sqrt{\pi}\sigma} \int_{0}^{\infty} \exp\left(\frac{-z^2}{2\sigma^2}\right) \left(1 - \frac{1}{p} \exp\left(\frac{-\sigma^2}{2\lambda_0^2}\right) + \frac{1}{p} \cos\frac{z}{\lambda_0}\right) \cos\frac{2\pi\nu z}{c} \mathrm{d}z \\ &= \exp\left(\frac{-2\pi^2\sigma^2\nu^2}{c^2}\right) + \frac{1}{p} \exp\left(-\frac{2\pi^2\sigma^2\nu^2}{c^2} - \frac{\sigma^2}{2\lambda_0^2}\right) \left(\cosh\frac{2\pi\sigma^2\nu}{c\lambda_0} - 1\right). \end{aligned}$$

The symmetry of $S(z)$ with respect to $z = 0$ and standard Fourier integrals from [Bro91] have been used. Searching now for zeros in the complex plane, i.e. $F(\nu) = 0$ for $\nu = \nu_\mathrm{r} + \mathrm{i}\nu_\mathrm{i}$, leads to

the condition

$$1 - p \exp\left(\frac{\sigma^2}{2\lambda_0^2}\right) = \cosh\frac{2\pi\sigma^2\nu}{c\lambda_0},$$

or, using the abbreviation $\alpha{=}2\pi\sigma^2/(c\lambda_0)$ and the relation $\cosh\alpha\nu{=}(e^{\alpha\nu}+e^{-\alpha\nu})/2$,

$$\begin{aligned} 2 - 2p\exp\left(\frac{\sigma^2}{2\lambda_0^2}\right) &= e^{\alpha(\nu_\mathrm{r}+\mathrm{i}\nu_\mathrm{i})} + e^{-\alpha(\nu_\mathrm{r}+\mathrm{i}\nu_\mathrm{i})} \\ &= e^{\alpha\nu_\mathrm{r}}\left(\cos\alpha\nu_\mathrm{i} + \mathrm{i}\sin\alpha\nu_\mathrm{i}\right) + e^{-\alpha\nu_\mathrm{r}}\left(\cos\alpha\nu_\mathrm{i} - \mathrm{i}\sin\alpha\nu_\mathrm{i}\right). \end{aligned}$$

The left-hand side of this equation is real, so

$$\begin{aligned} \left(e^{\alpha\nu_\mathrm{r}} - e^{-\alpha\nu_\mathrm{r}}\right)\sin\alpha\nu_\mathrm{i} &= 0 \\ \left(e^{\alpha\nu_\mathrm{r}} + e^{-\alpha\nu_\mathrm{r}}\right)\cos\alpha\nu_\mathrm{i} &= 2 - 2p\exp\left(\frac{\sigma^2}{2\lambda_0^2}\right) \le -\exp\left(\frac{-\sigma^2}{2\lambda_0^2}\right) \end{aligned} \tag{22}$$

must hold for any complex zero, where the inequality is due to the restriction Eq. (21).

Solutions for $\sin\alpha\nu_\mathrm{i}{=}0$ require thus $\cos\alpha\nu_\mathrm{i}{=}$-1 or $\alpha\nu_\mathrm{i} = (2m+1)\pi$ with m an integer, and additionally that the right-hand side of Eq. (22) is smaller than -2, as the minimum value of the sum in brackets on the right is +2. If this is fulfilled, then

$$\nu_\mathrm{r} = \frac{1}{\alpha}\ln\left(p\exp\left(\frac{\sigma^2}{2\lambda_0^2}\right)\left(1 \pm \sqrt{1 - \frac{2}{p}\exp\left(\frac{-\sigma^2}{2\lambda_0^2}\right)}\right) - 1\right). \tag{23}$$

In case the second term under the root is much smaller than unity, this expression can be simplified by expanding the root to first order for the positive sign or to second order for the negative sign, yielding

$$\nu_\mathrm{r} \approx \pm\left(\frac{c\lambda_0\ln 2p}{2\pi\sigma^2} + \frac{c}{4\pi\lambda_0}\right).$$

As an example, the oscillating Gaussian plotted in Fig. 5 has $\sigma{=}300\,\mu$m, $\lambda_0{=}20\,\mu$m and $p{=}10$, so that the approximation holds well and zeros occur for $\nu_\mathrm{r}{=}\pm1.2\,$THz. The Blaschke phase Eq. (15) for this case and its nonlinear contribution are plotted in Fig. 10. The first 2000 zeros in the negative complex plane were included in this calculation. Increasing the number of zeros further increases the phase itself, but does not change the nonlinear contribution significantly anymore. This behaviour was found in Sect. 3.3: zeros far away from the real axis contribute only linearly to the phase.

If the right-hand side of Eq. (22) lies between -2 and 0, Eq. (23) does not yield a real result. In this case zeros of the form factor are located on the imaginary axis, $\nu_\mathrm{r}{=}0$, at

$$\nu_\mathrm{i} = \pm\frac{1}{\alpha}\arccos\left(1 - p\exp\left(\frac{\sigma^2}{2\lambda_0^2}\right)\right) + \frac{2\pi m}{\alpha} \qquad \text{for any integer } m.$$

For every allowed parameter set σ, λ_0 and p there will therefore be either one or two values of ν_r for which an infinite number of zeros occur for values of ν_i given above.

Acknowledgments

Useful discussions with Evgeni Saldin, helping in clarifying several essential points, are greatly acknowledged.

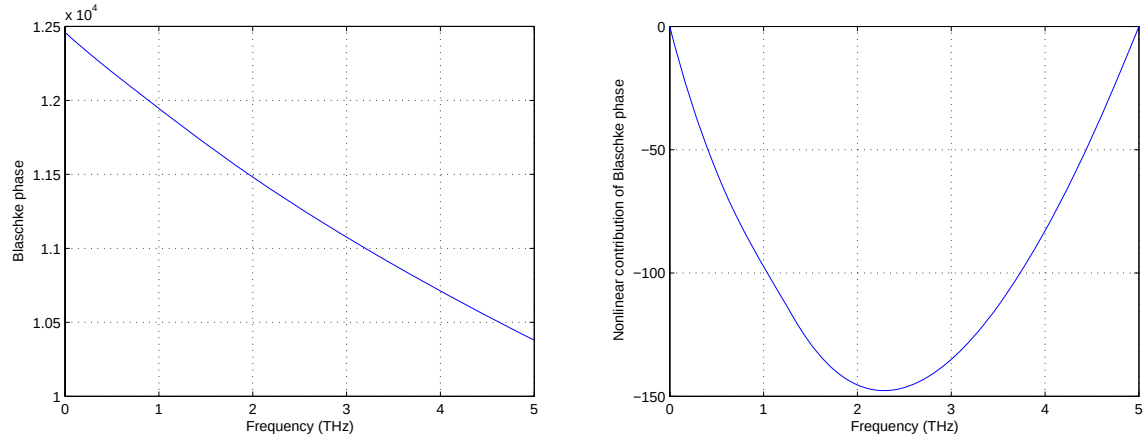

Figure 10 Blaschke phase (left) and its nonlinear contribution (right) for the oscillating Gaussian profile Eq. (20) with parameters σ=300 µm, λ_0=20 µm and p=10.

References

[Bro91] I.N. Bronstein, K.A. Semendjajew, *Taschenbuch der Mathematik*, B.G. Teubner (1991)

[Frö05] L. Fröhlich, *Bunch length measurements using a Martin-Puplett interferometer at the VUV-FEL*, DESY-THESIS 2005-011 (April 2005)

[Gel03] G. Geloni et al., *A method for ultrashort electron pulse-shape measurements using coherent synchrotron radiation*, DESY 03-031 (March 2003)

[Jack99] J. D. Jackson, *Classical Electrodynamics* (3rd edition), John Wiley & Sons, New York (1999)

[Lai97] R. Lai, A.J. Sievers, *On using the coherent far IR radiation produced by a charged-particle bunch to determine its shape: I Analysis*, Nucl. Instr. Meth. A397(1997) 221

[Men05] J. Menzel, *THz-Spektroskopie zur Bunchlängenmessung an der TESLA-Testanlage TTF*, DESY-THESIS 2005-012 (April 2005)

[Sal97] E.L. Saldin et al., *On the coherent radiation of an electron bunch moving in an arc of a circle*, Nucl. Instr. Meth. **A 398**, 373 (1997)

[Toll56] J.S. Toll, *Causality and the dispersion relation: Logical foundations*, Phys. Rev. **Vol. 104, No. 6**, 1760 (1956)

[Woo72] F. Wooten, *Optical properties of solids*, Academic Press (1972)